Real-time optical stabilization of retinal motion at micrometer precision using Adaptive Optics Flood-Illumination Ophthalmsocope

Pedro Mecê, Antoine Chen, Cyril Petit, Laurent Mugnier, Michel Paques, Serge Meimon

Real-time optical stabilization of retinal motion at micrometer precision using Adaptive Optics Flood-Illumination Ophthalmsocope

PEDRO MECÊ,[1,2,†,*] ANTOINE CHEN,[2,†] CYRIL PETIT,[2] LAURENT MUGNIER,[2] MICHEL PAQUES,[3] AND SERGE MEIMON[2]

[1] *Institut Langevin, ESPCI Paris, CNRS, PSL University, Paris, France*
[2] *DOTA, ONERA, Université Paris Saclay F-91123 Palaiseau, France*
[3] *Sorbonne Université, INSERM, CNRS, Institut de la Vision, Paris, France*
[†] *These authors equally contributed to this work.*
[*] *pedro.mece@espci.fr*

Abstract: Eye motion poses a significant challenge in efficiently capturing high-resolution retinal images and efficiently delivering cell-targeted photostimulation using adaptive optics (AO). In this manuscript, we present a solution to optically correct retinal movements in real-time by integrating galvanometer mirrors, pupil-conjugated, in an AO Flood-illumination ophthalmoscope (AO-FIO). Our approach involved using AO-FIO images to measure retinal motion with sub-pixel precision and correct it in a closed-loop fashion and at 200Hz. Through the proposed closed-loop optical stabilization, we achieved a notable reduction in retinal motion from 25 μm rms to 1.2μm rms. This performance was achieved 88% of the time over more than 40s without any decay of precision. Moreover, optical stabilization at this high precision was possible using images acquired in both photoreceptor and nerve fiber layers. To our knowledge, this level of precision and efficiency surpasses any previously reported method.

1. Introduction

Adaptive optics (AO) has become an important tool in ophthalmology due to its ability to correct ocular aberrations in real time [1]. AO technology has opened new avenues for earlier diagnosis and better treatment of retinal diseases, as well as a better understanding of the normal and diseased retina [2]. Indeed, applications such as cellular imaging of retinal neurons, super-resolution structured illumination [3], functional assessment by cell-targeted photostimulation [4], cellular psychophysical testing [5, 6], and high-precision laser photocoagulation surgery [7] benefit from AO's ability to achieve micrometer resolution. However, the improved spatial resolution afforded by the use of AO also makes these applications more sensitive to the effect of constant, involuntary eye movements, even during careful fixation [8, 9]. The main consequences of these fixational eye movements are 1) intra- and inter-frame distortion in point-scanning modalities such as scanning light ophthalmoscopy (SLO) and optical coherence tomography (OCT); 2) longer image acquisition sessions because some of the data is lost due to motion blur/distortion; and 3) inaccurate photostimulation, psychophysical testing, and photocoagulation. The consequences are even more critical in patients with retinal diseases or poor vision, as fixation eye motion is magnified, which severely limits the widespread use of AO technology in clinical settings. Therefore, to successfully achieve high-resolution imaging and precise delivery of visual stimuli to the retina in a clinical setting, it is critical to efficiently track and optically correct this motion in real time.

To date, closed-loop AO eye tracking systems have been developed primarily for AO-SLO. The first one used a tracking beam reflectometer to measure the displacement of the optic disc in real time and tip and tilt mirrors to optically stabilize the retinal motion [10]. Using this

method, the authors demonstrated a tracking accuracy of 10-15μm. However, this system has important limitations in terms of stability and robustness, as it requires significant tuning of parameters and settings for each eye. Furthermore, the achieved accuracy was not sufficient to eliminate intra- and inter-frame motion distortions in AO-SLO images. Later, Yang *et al.* showed that closed-loop image-based optical stabilization can be achieved in an AO-SLO by replacing the slow scanner mirror with a 2-axis tip/tilt mirror and using AO-SLO images for motion measurement [11]. Their method achieved very good efficiency (85%) and accuracy of $\sim 1.66\mu m - 2.56\mu m$ (an order of magnitude better than the previous work). Nevertheless, their optical stabilization technique suffers from the inherent limitations of an AO SLO, the most important of which are 1) intra-frame distortion in the reference frame encoded in the optical stabilization; 2) tracking failure due to large amplitude motion and eye torsion; 3) decrease in tracking efficiency with increasing imaging duration (20-30 seconds in duration) due to subject fatigue and eye torsion; 4) and difficulty in resetting the position of the tracking mirror after micro-saccades, blinks, frame-outs, and torsions occur. All of these limitations are a major problem for clinical imaging, where motion is amplified, subjects tend to fatigue more quickly, and longer acquisition sessions are typically required.

In contrast to point-scanning modalities, there are full-field modalities, such as AO flood-illumination ophthalmoscope (FIO) [12] and full-field OCT [13]. These full-field modalities are distortion-free due to their high pixel rate, which combines a short exposure time with full-field illumination and detection. AO-FIO images are often used as ground truth to evaluate the ability of image registration methods to minimize distortion in AO-SLO, and also to validate photoreceptor-based biomarkers extracted from AO-SLO images [14]. In addition, full-field modalities allow combining a high acquisition rate with a large field of view [12], parameters that together can play an important role in achieving high-precision and high-efficiency optical stabilization of retinal motion in real time.

However, the main challenge of using an AO-FIO to track and correct for fixation eye movements lies in the fact that the AO-FIO does not have optical sectioning capability [15]. Multiple scattered light and light backscattered by out-of-focus retinal layers are all detected in AO-FIO, making its image contrast and SNR worse than AO-SLO. Due to the low SNR and poor contrast, the eye motion estimation methods currently used in AO-SLO, which are based on simple cross-correlations, tend to fail in AO-FIO [11, 16]. To overcome this inherent drawback of AO-FIO images, several methods have been proposed, the most successful being Maximum-Likelihood estimation [17] and Peak Tracking [18]. However, although these methods allow for subpixel motion estimation, they are time-consuming and not compatible with the application of real-time optical stabilization of eye movements.

To explore the advantage of full-field modalities, i.e., high-throughput, distortion-free, and large FOV images, we present here, for the first time, an AO-FIO designed to provide real-time optical stabilization of retinal motion. To mitigate the low image contrast and SNR, and to estimate the eye motion with precision at the millisecond scale, we propose a method based on phase correlation of high spatial frequencies. Although AO-FIO has no optical sectioning, high spatial frequencies are generated only by the retinal layer within the depth of focus [15]. By relying on the cross-correlation of these frequencies and filtering out low and noisy spatial frequencies, one can minimize the noise error propagation in motion estimation. With this method, and without the use of special integrated circuits such as field-programmable gate arrays (FPGAs) and graphics processing units (GPUs) previously required in AO-SLO methods, we can measure the lateral retinal displacement in the millisecond range and with sub-pixel (sub-micrometer) precision, thus allowing robust correction of eye movements during the imaging session with micrometer precision.

2. Methods

2.1. Experimental set-up

The AO-FIO system with robust closed-loop optical stabilization can be decomposed in three subsystems: the imaging, the wavefront sensing/correction, and the eye motion tracking/correction subsystems (see Fig. 1).

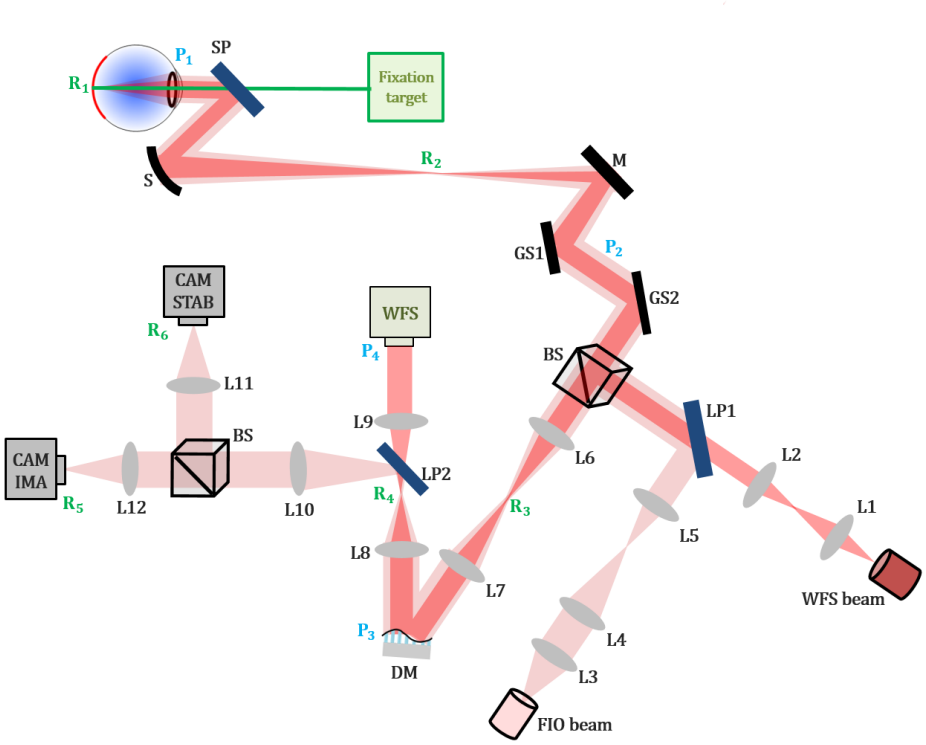

Fig. 1. Synoptic schema of the Adaptive Optics-Flood Illumination Ophthalmoscope set-up. The system can be divided into three main systems: wavefront sensing and correction part at 750 nm (dark red beam path), the imaging part with CAM IMA and the eye motion trackng and correction subsystem. (L stands for lenses and doublets, BS for beamsplitters, R for focal/retinal planes, P for pupil planes).

Imaging subsystem. A SLD (LedMOD.850.800.V2, Omicron, Germany with a central wavelength of 860nm (100nm bandwidth) is used as illumination source. A squared field diaphragm is positioned at the retinal plane R_7, which defines an illumination field of view in the retina of $4^o \times 4^o$. The light backscattered by the retina is split in half by a beam splitter and then captured by two scientific CMOS cameras (ORCA flash4-v2, Hamamatsu, Japan), each one with a different purpose. The first one, the imaging camera, enables a large field-of-view imaging at diffraction-limited resolution. It can reach 200Hz while acquiring 1024×1024 pixel per frame, corresponding to approximately $4^o \times 4^o$ in the retina. This camera is mounted on a motorized stage, enabling focusing on different retinal layers. The second camera, the stabilization camera, provides a small field-of-view and undersampled resolution, for faster computation of eye motion. Images of 512×512 pixel ($4^o \times 4^o$ field of view) are acquired at 200Hz. Although a faster acquisition rate would be possible for the stabilization camera, a 5ms exposure time was necessary

to precisely measure eye motion and beat the noise level, which is high in an AO-FIO system.

Wavefront sensing/correction: A fibered SLD (EXS210017-01, Exalos, Swiss) with a central wavelength of 750nm is used as a wavefront sensor beacon. The size of the beacon at the eye pupil is $277\mu m$, which is defined by a mask positioned at a pupil plane of the wavefront sensor beacon. The beacon is offset by two 2cm in the eye's pupil to prevent stray light. Wavefront sensing is performed using a custom-built Shack-Hartmann sensor consisting of a 18 × 18 microlens array (MLA300-14AR-M, Thorlabs, USA). Relay optics conjugate the focal plane of the microlenses onto a CMOS camera (UI-3360CP-NIR-GL Rev.2, IDS, Germany), where 16 × 16 pixels are allocated to each lenslet. The pitch of the microlens array corresponds to $278\mu m$ in the eye pupil plane. Wavefront correction is performed by a deformable mirror with 97 actuators (ALPAO, France). The deformable mirror diameter limits the pupil size of the system to 5mm. The deformable mirror can also be used to change the focal plane of both detectors during imaging and optical stabilization of eye motion. To control the adaptative optics, we used our custom-built real-time calculator (RTC), allowing us to achieve a 50Hz loop rate without jitter. We applied an integrator control law with a 0.5 gain, assuming a two-frame delay.

Eye motion tracking/correction: Two galvanometer mirrors are positioned very close to the pupil plane P_2 and responsible for correcting eye motion in real-time. Both illumination and wavefront sensor beacon beams pass by the galvanometers, on the way towards the retina and from the retina towards the detectors. An independent custom-built RTC, written in Matlab (MathWorks, Natick, MA), was used to measure eye motion through the images provided by the stabilization camera. No particular integrated circuit, such as field-programmable gate array (FPGA) or graphics processing units (GPU), was used, but rather a CPU (Core i7 - 4790K). Eye motion correction is performed at a 200Hz loop rate without jitter. As for AO, the control law is an integrator with a 0.5 gain, with a two-frame delay chronogram (see Fig.2).

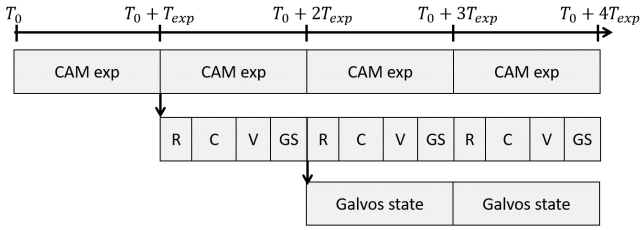

Fig. 2. Breakdown of the eye motion optical stabilization loop chronogram. After acquiring an image during the camera exposure time T_exp, the image is read by the computer (R), the eye motion is computed (C) the corresponding voltage is estimated (V) and sent to the galvanometer scanners with a given response time (GS). Correction is thus applied in the galvanometer scanners after two frames from the start of the image acquisition.

2.2. Eye motion tracking algorithm and control loop

The tracking algorithm is image-based and relies on the rapid matching of an acquired reference frame and an acquired frame. The algorithm can be divided into two main parts: selection of the appropriate reference frame and estimation of eye movement by comparing the reference and acquired frames. In this study, the reference frame was automatically chosen as the first acquired frame of the sequence without any blink and micro-saccade occurrence (see the blink

and micro-saccade detection method below). We then compute the Fast Fourier Transform (FFT) of the reference frame and apply a bandpass filter to filter out the low spatial frequency (dominated by photons collected from out-of-focus retinal layers and multiply scattering) and the high spatial frequency (dominated by photon noise) of the image. For the bandpass filter, we used a Butterworth of order 2 with normalized cut-off frequencies of 0.01 and 0.5. The normalized cut-off frequencies were chosen based on a parametric study described in Supplement 1. After this step, the algorithm is ready to start the real-time optical stabilization. First, the same reference frame procedure is applied to the acquired frames, *i.e.* FFT computation and bandpass filtering with the same parameters. Then a phase correlation is performed by multiplying the reference filtered FFT with the acquired filtered FFT. By taking the real part, one can obtain a correlation map where the 2D position of the maximum value provides the shift between the two images. Finally, sub-pixel estimation is performed by computing a parabolic fit of pixels surrounding the maximum position in the horizontal and vertical directions. Here, 5 pixels were used for each direction. From the parabolic fit, a new maximum can be found with sub-pixel precision.

Based on our parametric study described in Supplement 1, we decided to work with an undersampled stabilization camera where the pixel size in the retinal plane is $2.36\mu m$ while the diffraction limit is $2.9\mu m$. Undersampling by a factor of two allows: 1) increase the SNR by a factor of two, 2) reduce the computation time by a factor of about 2.22 (FFT computation complexity equal to $nlogn$, where n is the number of the data size). Undersampling could come at the cost of lower motion estimation accuracy. However, since the motion estimation precision is on the order of a tenth of a pixel (subpixel precision), the loss is not significant compared to the temporal error introduced by the 2-frame delay loop. To further reduce the computation time, we only acquire images of 128×128 pixels (about $1^o \times 1^o$ FOV), which allows us to achieve a computation time of 2.5ms including image transfer and motion estimation in a CPU (Core i7 4790K). The FOV was chosen to avoid frame-out, which can occur after micro-saccades, based on eye movement data collected without correction (peak-to-valley value in table 1). After estimating the eye movement, we calculate the voltage needed to drive the galvanometers and correct for this movement. Voltage calculation and response time of the galvanometer mirrors is typically 2ms, which allows the use of a two-frame delay control loop chronogram (see Fig. 2) with 5ms exposure time for the stabilization camera, i.e. at 200Hz loop rate.

Blinks and micro-saccades can be a potential source of control instability during eye movement correction [11]. Here, to avoid instability during and after blinks and micro-saccades occur, we keep the galvanometer state at the same position just before they occur. Blinks are detected by an image intensity threshold. Micro-saccades are detected by computing the integral of the FFT of the filtered image [19], which allows us to evaluate the energy associated with the high spatial frequencies of the in-focus structure of the retina. In fact, during micro-saccades, the AO-FIO images lose high spatial frequencies due to image blur. Once detected, the loop is reactivated only when the difference between two successive motion estimates is less than $2\mu m$.

2.3. Image acquisition

We acquired images from three healthy subjects. Participants followed institutional guidelines and adhered to the tenets of the Declaration of Helsinki. Informed consent was obtained from the participants after the natural and possible outcomes of the study were explained. The participants were seated in front of the system and stabilized with a chin and forehead rest. The participants were asked to stare at the fixation target, which is an image of a yellow cross not affected by the optical sectioning, enabling guiding the subject's line of sight and exploring various areas of the retina. Image acquisition sessions were performed in standard conditions with neither pupil dilation nor cycloplegia, in a dark room, leading to the largest accessible natural pupil dilation. The total light energy entering the eye from the illumination source and the wavefront sensor

beacon source were, respectively, 3mW and $6\mu W$, which is less than the limits established by ISO standards for group 1 devices.

3. Results

3.1. Closed-loop optical stabilization internal performance

The overall system temporal performance of a control loop can be assessed and optimized by computing its rejection transfer function (or sensitivity function) [20, 21]. The rejection transfer function describes how different eye motion temporal frequencies are attenuated or amplified by the closed-loop optical stabilizer. From this function, one can also assess the correction cutoff frequency, *i.e.* the highest corrected temporal frequency. To compute the rejection transfer function, we injected in the galvanometer mirrors a pink noise with a power spectrum density following an f^{-1} law (this type of colored noise avoids applying too much energy at high temporal frequencies that could degrade the galvanometer mirrors). Eye motion is then estimated in a model eye with correction (loop on, *i.e.* residual eye motion) and without correction (loop off). The rejection transfer function is the ratio between temporal power spectral densities of the residual eye motion (*i.e.* with correction) and eye motion (*i.e.* without correction). Figure 3 shows the experimental computed rejection transfer function (blue: horizontal, green: vertical) and the theoretical one (red line) assuming a two-frame delay and 0.5 gain (which are the actual settings used during the acquisition). The good match between the experimental and theoretical plots demonstrates that no additional delay or jitter was present during the acquisition, meaning that the temporal performance of the loop is as expected. In our case, with a 200Hz loop rate, the cutoff frequency (associated with 0dB) is approximately 14Hz.

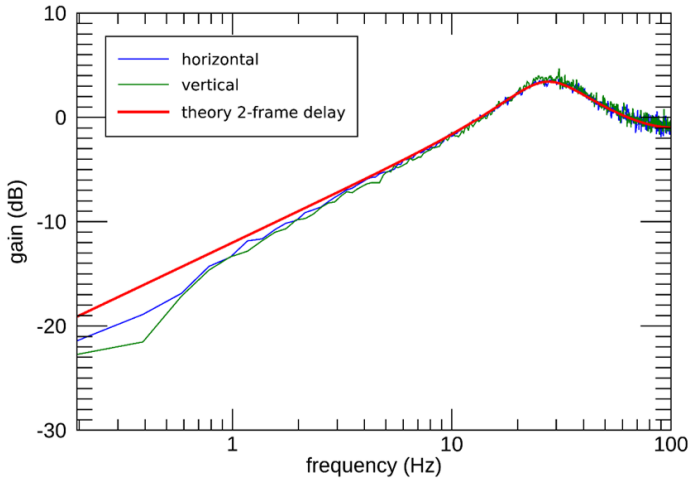

Fig. 3. Rejection Transfer function. Blue and green: experimental rejection transfer function on horizontal and vertical directions respectively. Red: theoretical rejection for a 2-frame delay loop.

3.2. Performance of the retinal lateral motion optical stabilization

Figure 4(a,b) presents an example of vertical (Y) and horizontal (X) retinal displacement as a function of time. Here, the stabilization camera was conjugated to the photoreceptor layer focal plane, and the loop rate was set to 200Hz. During the first 5 seconds (red line), no correction was applied. Slow drifts, and fast and large amplitude micro-saccades were visible in both

X,Y directions. After activating the closed-loop optical stabilization (final 5 seconds), slow drifts were completely filtered out (blue line). On the other hand, micro-saccades were not fully corrected (black line). Note that, owing to the real-time detection of micro-saccades and blink occurrences, the closed-loop correction is barely affected by these spark movements and can robustly re-active the closed-loop correction very fast after these occurrences, achieving high efficiency. Visualization 1 shows the images acquired by the stabilization camera before and after correction of eye motion in real-time. As a reminder, the images acquired by the stabilization camera are those used to measure the retina position in real-time, i.e. undersampled.

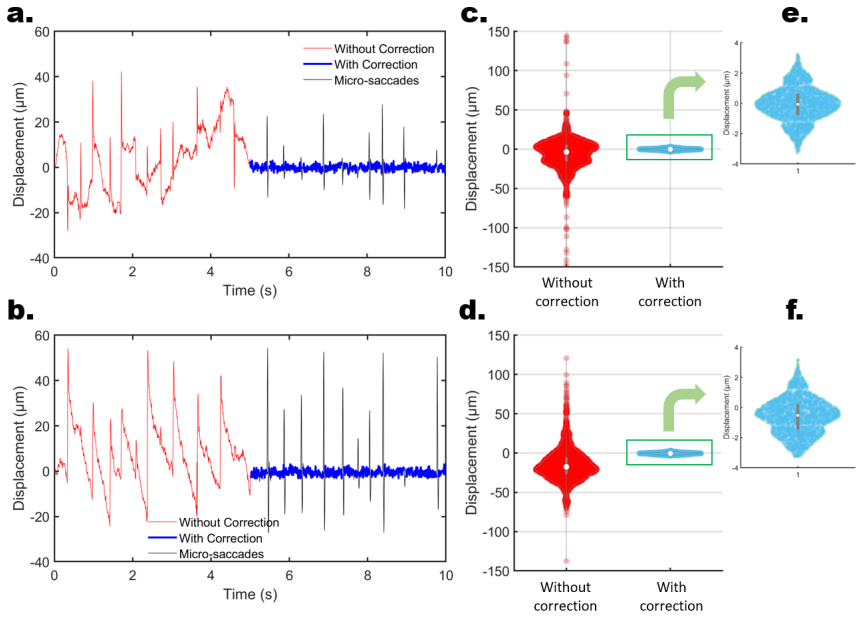

Fig. 4. (a,b) Example of retinal displacement over time in the vertical (Y) and horizontal (X) directions respectively. (c,d) Distribution of displacements without and with correction of retinal motion collected from a 40-s long data set, where the first 20s seconds are without correction, and the final 20s with correction (i.e. 4000 time points for each case). (e,f) is the magnified plot when correction was activated to better visualize its distribution.

Figure 4(c,d) shows the distribution of displacements without and with correction of retinal motion collected from a 40-s long data set, where the first 20s seconds are without correction, and the final 20 s with correction (*i.e.* 4000 time points for each case). Figure 4(e,f) is the magnified plot when correction was activated, highlighting the high precision achieved. When retinal motion is not corrected, we computed a peak-to-valley amplitude X,Y of respectively 258.35μm and 290.98μm , a mean deviation from zero position X,Y of respectively 20.6μm and 13.13μm, and a root-mean-square (RMS) error X,Y of respectively 24.78μm and 18.29μm. On the other hand, the proposed closed-loop optical stabilization system reduced the peak-to-valley amplitude X,Y to respectively 6.49μm and 6.56μm , the mean deviation from zero position X,Y to respectively 1.05μm and 0.9μm, and the root-mean-square (RMS) error X,Y to respectively 1.19μm and 1.15μm. Table 1 summarizes the achieved performance with the proposed method.

During the eye motion correction in real-time using the images acquired by the stabilization camera, the imaging camera acquires in parallel large field-of-view images of the retina. Since these cameras are independent, it is possible to position the focal plane at different layers. For

	PV (μm)	Mean deviation (μm)	RMS error (μm)
Without correction	$X : 258.35, Y : 290.98$	$X : 20.6, Y : 13.13$	$X : 24.78, Y : 18.29$
With correction	$X : 6.49, Y : 6.56$	$X : 1.05, Y : 0.9$	$X : 1.19, Y : 1.15$

Table 1. Axial motion statistics with and without optical stabilization of retinal motion. Statistics took into account 40-s long data set, where the first 20s seconds are without correction, and the final 20s with correction (i.e. 4000 time points for each case). PV stands for peak-to-valley amplitude.

example, the stabilization camera could be focused to the photoreceptor layer while the imaging camera acquires images from the nerve fiber layer. Visualization 2,3 show the images acquired without any correction and during the real-time eye motion correction, respectively, in the nerve fiber layer. Figure 5(a,b) presents the result of averaging 400 images (4 s acquisition) without and with eye motion correction in real-time. One can noticed that owing to the optical stabilization of eye movements, the high spatial content in the NFL is maintained while it is totally vanished when no eye motion correction is applied. Figure 5(c) shows the result of averaging 400 images after a post-processing digital correction of eye motion, thus without considering the temporal error added by the real-time control loop. Since the precision obtained with the optical stabilization method is below the size of a single pixel, the averaged image obtained after post-processing registration is very similar to the one obtained with real-time correction, without any apparent loss of high-spatial frequency content of the nerve fiber layer.

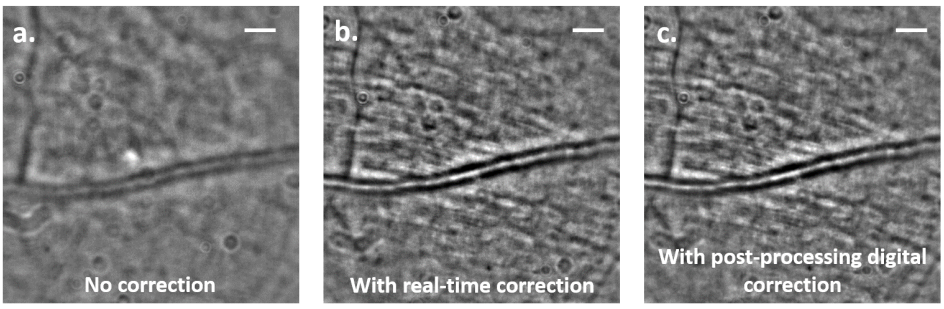

Fig. 5. Result of averaging 400 images acquired by the imaging camera (a) before and (b) during real-time optical stabilization of eye movements.(c) Result of averaging 400 images acquired by the imaging camera during real-time optical stabilization of eye movements and further post-processing image registration at sub-pixel precision. Scale bar 100μm.

3.3. Performance for different stabilization camera focal planes

To achieve precise optical stabilization on an image-based method, one needs to collect images with high spatial frequency content to enhance the precision of cross-correlation methods. High-spatial frequency content can be found when imaging the photoreceptor layer, and it was, so far, the only retinal layer explored to demonstrate eye motion optical stabilization [11]. However, it is not rare in patients that the photoreceptor layer is not sharply imaged or partially/completely absent because of the pathological retinal condition, in particular for age-related macular degeneration and diabetic retinopathy. For these cases, it is crucial to demonstrate that closed-loop optical

stabilization can precisely track eye motion based on images generated in other retinal layers. Owing to our system design based on two independent cameras, one can conjugate the stabilization camera in one specific retinal layer while imaging another one. Another retinal layer that presents relatively high spatial frequency is the nerve fiber layer. Table 2 presents a comparison of the performance of the proposed method while conjugating the stabilization camera in the photoreceptor and the nerve fiber layers. Visualization 4 presents a video acquired by the stabilization camera during real-time eye motion correction while focused on the nerve fiber layer.

	Tracked Frames	Failed Frames	Efficiency	RMS error
Photoreceptor layer	19067	2269	88.1%	$1.32\mu m$
Nerve fiber layer	20197	2444	87.8%	$1.48\mu m$

Table 2. Axial motion statistics with and without the use of the method to optically stabilize retinal axial motion. Statistics took into account 13 image sequences of 7 to 28s duration from three subjects, for a total of 4700 analyzed A-scans. PV stands for peak-to-valley amplitude.

Note that both conditions presented very high and comparable efficiency, around 88%. Moreover, both scenarios revealed high tracking precision, slightly better for the photoreceptor layer ($1.32\mu m$) than the nerve fiber layer ($1.48\mu m$). This result shows that both retinal layers could be used to precisely track and correct eye motion in real-time with the proposed method.

3.4. Stabilization precision and efficiency over time

Using an AO-SLO system to execute a closed-loop image-based optical stabilization, Yang *et al.* noticed in their 20 to 30-second long tracking data that the tracking efficiency decreases as imaging duration increases [11]. They associated this phenomenon with subject fatigue due to the long imaging time, increasing eye motion amplitude. To evaluate how our system efficiency and precision evolved, we acquired 40s long data while the closed-loop optical stabilization was activated. The stabilization camera was conjugated to the nerve fiber layer focal plane, and the loop rate was running at 200Hz. Figure 6(a) shows the horizontal retinal displacement over time, where the blue plot represents the time points where the correction was activated and the red plot where micro-saccades or blink occurrences were detected. No significant increase of micro-saccades was detected in this time series. On the other hand, Fig.6 (b) shows an increase in the mean deviation from zero retinal displacement over time, supporting the hypothesis that the longer the imaging duration, the larger the retinal motion. However, in contrast to Yang *et al.* results, here both efficiency and precision do not present a decrease over time (see Fig.6(c)). Efficiency was highly correlated to the occurrences of micro-saccades and blinks. The steady precision and efficiency in our case, in contrast to the AO-SLO method [11], may be explained by the use of large FOV and distortion-free images. Another explanation can be the fact that while image rotation, provoked by eye torsion, does not affect motion estimation in AO-FIO, it makes AO-SLO image-based registration methods to fail or loose their precision [11].

4. Discussion and Conclusion

In this manuscript, we have presented an AO-FIO imaging system that is capable of optically stabilizing the lateral motion of the retina in real-time. We have shown that a loop rate of 200 Hz can be achieved with a temporal bandwidth of 14 Hz, eliminating all slow drifts and being immune to micro-saccades and blinks. Due to the ability of the AO-FIO to generate distortion-free

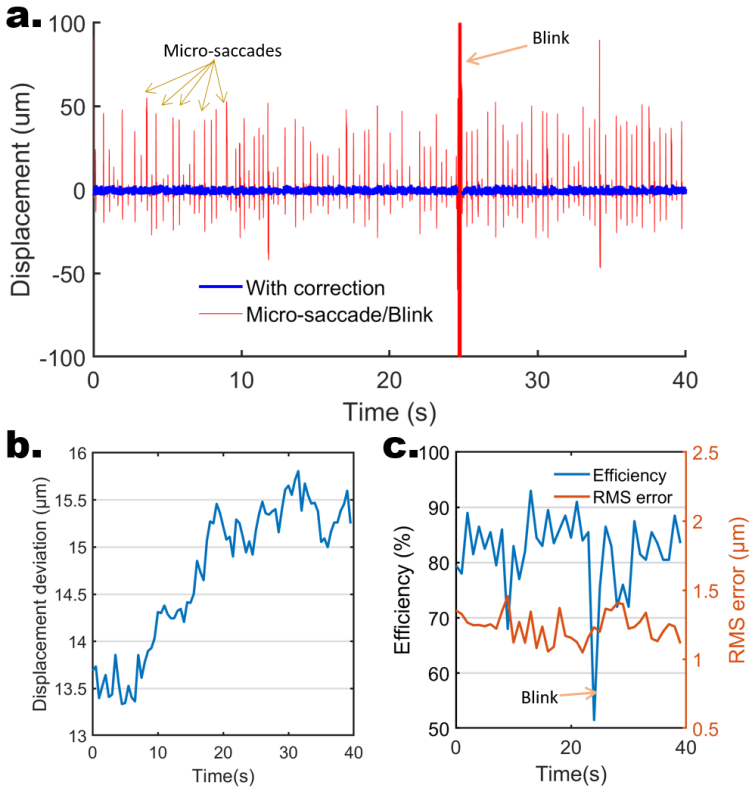

Fig. 6. Evaluation over time of the precision and efficacy of the proposed optical stabilization method to correct for eye motion in real-time. (a) Retinal displacement over time during real-time optical stabilization. Red traces outline high amplitude and spark motion due to micro-saccades and one blink occurrence around 25s. (b) Mean deviation from zero of the retinal displacement over time. (c) Efficiency and RMS error over time.

images over a large FOV, optical stabilization was successful in all experiments. Our proposed optical stabilization method reduced retinal motion from $25\mu mRMS$ to $1.2\mu mRMS$, *i.e.* less than the distance between foveal photoreceptors. This performance was achieved 88% of the time for a total of 39264 acquired images. The 12% of unsuccessful tracking was mainly due to the occurrence of micro-saccades and blinks, which can be accurately detected. Due to the detection of blinks and micro-saccades, the control loop is deactivated to avoid instability, and reactivated when a normal state is reached again. To the best of our knowledge, the performance achieved by the proposed method is more precise and efficient than any other method reported in the literature. Moreover, in contrast to the previous work by Yang et al. [11], such precision and efficiency was possible without using any special integrated circuit, such as field-programmable gate arrays (FPGA) or graphics processing units (GPU), but a CPU (7 - 4790K).

The use of FPGA and GPU can increase the efficiency/robustness of the proposed method by increasing the field of view of the stabilization camera (while keeping the loop rate at 200 Hz), especially in patients with large fixational eye movements or poor vision or even nystagmus. Another advantage of using FPGA and GPU is the possibility to increase the loop rate even more. In fact, in this study, the loop rate was limited by the image processing time. In Supplement 1, we

show that the proposed algorithm could still estimate eye movements with sub-micro precision in images with a SNR 3 times lower than the one used, i.e. an exposure time of 1.67 ms. Another interesting advantage of the proposed method, demonstrated for the first time, is its ability to achieve precise eye motion correction even when the images were acquired in a retinal layer other than the photoreceptors. Here, we obtained equivalent precision and efficiency when using images acquired in both the photoreceptors and the nerve fiber layer. In fact, this advantage can be very helpful when imaging patients for whom it is difficult to obtain a clear and sharp image of the photoreceptors (e.g., patients with age-related macular degeneration or drusen). Contrary to the previous work by Yang et al. using AO-SLO images to track eye movements [11], no decrease in efficiency over time was observed, most likely because all pixels are collected at the same time in a large FOV, avoiding frame-out errors and uncertainties due to motion-induced distortion and eye torsion (provoking image rotation). Finally, the performance in terms of precision and efficiency can be further improved if the reference image has a better SNR than the current images (see Supplement 1). Indeed, this can be achieved as a first step, where acquiring, registering and averaging 25 images and using the averaged image as a new reference could potentially increase the precision of eye motion estimation by a factor of 5 for the same image SNR used in this study (5ms exposure), or by allowing precise estimation in even noisier images with a shorter exposure time, thus potentially allowing a faster loop rate (see Supplement 1).

The performance achieved in this study opens a new avenue in terms of applications, especially in subjects with retinal pathology. With the presented performance, one has the tools to image patients who are potentially the most interesting to study with AO ophthalmoscopes, such as nystagmus patients or patients with poor fixation capacity due to poor vision. In addition, precise delivery of visual stimuli for photostimulation or laser strikes for photocoagulation surgery may be possible in patients with poor fixation. Furthermore, the proposed algorithm, which is robust to noisy images, can be used to estimate eye movements during psychophysical testing and may help to find early signs of retinal diseases by characterizing fixational eye movements [6]. Finally, other full-field modalities that need to mitigate eye movements to be successful, such as DMD-based partial-field and camera-based multimodal ophthalmoscopes [22, 23], Structured Illumination Ophthalmoscope [3] and Full-Field Optical Coherence Tomography [24], could greatly benefit from the proposed optical stabilization method.

5. Backmatter

Funding. Agence Nationale de la Recherche (ANR-18-IAHU-0001, ANR-22-CE19-0010-01, ANR-18-CE19-0010, ANR-15-RHUS-0001) ONERA's internal project PRF TELEMAC.

Disclosures. PM: ONERA (P), AC: Quantel Medical (E), CP: ONERA (P), and SM: ONERA (P).

Data availability. Data underlying the results presented in this paper are not publicly available at this time but may be obtained from the authors upon reasonable request.

Supplemental document. See Supplement 1 for supporting content.

References

1. J. Liang, D. R. Williams, and D. T. Miller, "Supernormal vision and high-resolution retinal imaging through adaptive optics," JOSA A **14**, 2884–2892 (1997).
2. J. I. Morgan, T. Y. Chui, and K. Grieve, "Twenty-five years of clinical applications using adaptive optics ophthalmoscopy," Biomed. Opt. Express **14**, 387–428 (2023).
3. Y. Lai-Tim, L. Mugnier, L. Krafft, A. Chen, C. Petit, P. Mecê, K. Grieve, M. Paques, and S. Meimon, "Super-resolution in vivo retinal imaging using structured illumination ophthalmoscopy," arXiv preprint arXiv:2007.16028 (2020).
4. F. Zhang, K. Kurokawa, A. Lassoued, J. A. Crowell, and D. T. Miller, "Cone photoreceptor classification in the living human eye from photostimulation-induced phase dynamics," Proc. Natl. Acad. Sci. **116**, 7951–7956 (2019).
5. J. L. Reiniger, N. Domdei, F. G. Holz, and W. M. Harmening, "Human gaze is systematically offset from the center of cone topography," Curr. Biol. **31**, 4188–4193 (2021).

6. J. Murari, J. Gautier, J. Daout, L. Krafft, P. Senee, P. Mece, W. Seiple, K. Grieve, D. Sheynikhovich, S. Meimon *et al.*, "Foveal drusen increase fixation instability: fixational eye movements as biomarkers for pre-symptomatic amd," bioRxiv pp. 2023–10 (2023).
7. P. B. de Mecê, "4d exploration of the retina for adaptive optics-assisted laser photocoagulation," Ph.D. thesis, Université Sorbonne Paris Cité (2018).
8. S. Martinez-Conde, S. L. Macknik, and D. H. Hubel, "The role of fixational eye movements in visual perception," Nat. reviews neuroscience **5**, 229–240 (2004).
9. P. Mecê, J. Jarosz, J.-M. Conan, C. Petit, K. Grieve, M. Paques, and S. Meimon, "Fixational eye movement: a negligible source of dynamic aberration," Biomed. optics express **9**, 717–727 (2018).
10. R. D. Ferguson, Z. Zhong, D. X. Hammer, M. Mujat, A. H. Patel, C. Deng, W. Zou, and S. A. Burns, "Adaptive optics scanning laser ophthalmoscope with integrated wide-field retinal imaging and tracking," JOSA A **27**, A265–A277 (2010).
11. Q. Yang, J. Zhang, K. Nozato, K. Saito, D. R. Williams, A. Roorda, and E. A. Rossi, "Closed-loop optical stabilization and digital image registration in adaptive optics scanning light ophthalmoscopy," Biomed. optics express **5**, 3174–3191 (2014).
12. E. Gofas-Salas, P. Mecê, C. Petit, J. Jarosz, L. M. Mugnier, A. M. Bonnefois, K. Grieve, J. Sahel, M. Paques, and S. Meimon, "High loop rate adaptive optics flood illumination ophthalmoscope with structured illumination capability," Appl. optics **57**, 5635–5642 (2018).
13. J. Scholler, K. Groux, K. Grieve, C. Boccara, and P. Mecê, "Adaptive-glasses time-domain ffoct for wide-field high-resolution retinal imaging with increased snr," Opt. Lett. **45**, 5901–5904 (2020).
14. A. E. Salmon, R. F. Cooper, C. S. Langlo, A. Baghaie, A. Dubra, and J. Carroll, "An automated reference frame selection (arfs) algorithm for cone imaging with adaptive optics scanning light ophthalmoscopy," Transl. vision science & technology **6**, 9–9 (2017).
15. P. Mecê, E. Gofas-Salas, M. Paques, K. Grieve, and S. Meimon, "Optical incoherence tomography: a method to generate tomographic retinal cross-sections with non-interferometric adaptive optics ophthalmoscopes," Biomed. optics express **11**, 4069–4084 (2020).
16. M. Zhang, E. Gofas-Salas, B. T. Leonard, Y. Rui, V. C. Snyder, H. M. Reecher, P. Mecê, and E. A. Rossi, "Strip-based digital image registration for distortion minimization and robust eye motion measurement from scanned ophthalmic imaging systems," Biomed. Opt. Express **12**, 2353–2372 (2021).
17. D. Gratadour, L. M. Mugnier, and D. Rouan, "Sub-pixel image registration with a maximum likelihood estimator-application to the first adaptive optics observations of arp 220 in the l band," Astron. & Astrophys. **443**, 357–365 (2005).
18. G. Ramaswamy and N. Devaney, "Pre-processing, registration and selection of adaptive optics corrected retinal images," Ophthalmic Physiol. Opt. **33**, 527–539 (2013).
19. P. Mecê, E. Gofas-Salas, C. Petit, F. Cassaing, J. Sahel, M. Paques, K. Grieve, and S. Meimon, "Higher adaptive optics loop rate enhances axial resolution in nonconfocal ophthalmoscopes," Opt. letters **44**, 2208–2211 (2019).
20. F. Roddier, *Adaptive Optics in Astronomy* (Cambridge University Press, 1999).
21. P. Mecê, J. Scholler, K. Groux, and C. Boccara, "High-resolution in-vivo human retinal imaging using full-field oct with optical stabilization of axial motion," Biomed. Opt. Express **11**, 492–504 (2020).
22. L. Krafft, E. Gofas-Salas, Y. Lai-Tim, M. Paques, L. Mugnier, O. Thouvenin, P. Mecê, and S. Meimon, "Partial-field illumination ophthalmoscope: improving the contrast of a camera-based retinal imager," Appl. optics **60**, 9951–9956 (2021).
23. L. Krafft, P. Senée, E. Gofas, O. Thouvenin, M. Atlan, M. Paques, S. Meimon, and P. Mecê, "Multimodal high-resolution retinal imaging using a camera-based dmd-integrated adaptive optics flood-illumination ophthalmoscope," Opt. Lett. **48**, 3785–3788 (2023).
24. P. Mecê, J. Scholler, K. Groux, K. Grieve, and C. Boccara, "Adaptive glasses wavefront sensorless full-field oct for high-resolution retinal imaging over a wide field-of-view," in *Ophthalmic Technologies XXXI,* vol. 11623 (SPIE, 2021), p. 1162306.